

# A Singlet-Diradical Co(III)-Dimer as a Nonvolatile Resistive Switching Device: Synthesis, Redox-Induced Interconversion, and Current–Voltage Characteristics

Suman Sinha,<sup>#</sup> Muhammed Sahad E,<sup>#</sup> Rakesh Mondal,<sup>#</sup> Siuli Das, Litty Thomas Manamel, Paula Brandão, Bas de Bruin, Bikas C. Das,<sup>\*</sup> and Nanda D. Paul<sup>\*</sup>



Cite This: *J. Am. Chem. Soc.* 2022, 144, 20442–20451



Read Online

ACCESS |



Metrics & More

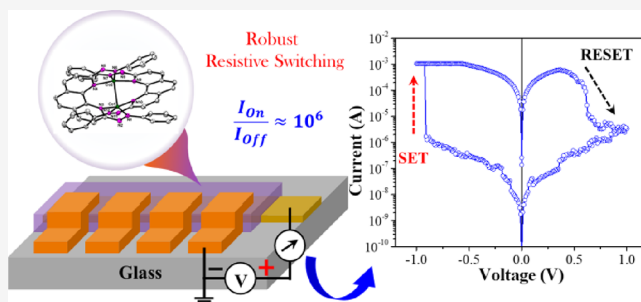


Article Recommendations



Supporting Information

**ABSTRACT:** Herein we report a ligand-centered redox-controlled strategy for the synthesis of an unusual binuclear diradical cobalt(III) complex,  $[\text{Co}_2^{\text{III}}(\text{L}^{\bullet 3-})_2]$  (**1**), featuring two three-electron reduced trianionic monoradical 2,9-bis(phenyldiazo)-1,10-phenanthroline ligands ( $\text{L}^{\bullet 3-}$ ) and two intermediate-spin cobalt(III) centers having a Co–Co bond. Controlled ligand-centered oxidation of **1** afforded two mononuclear complexes,  $[\text{Co}^{\text{II}}(\text{L}^{\bullet -})(\text{L}^0)]^+$  ( $[\mathbf{3}]^+$ ) and  $[\text{Co}^{\text{II}}(\text{L}^0)_2]^{2+}$  ( $[\mathbf{2}]^{2+}$ ), which upon further ligand-centered reduction yielded a di-azo-anion diradical complex,  $[\text{Co}^{\text{II}}(\text{L}^{\bullet -})_2]$  (**4**). In complex **1**, two three-electron reduced di-azo-anion monoradical ligands ( $\text{L}^{\bullet 3-}$ ) bridge two intermediate Co(III) centers at a distance of 2.387(2) Å, while upon oxidation, one of the coordinating azo-arms of **L** becomes pendent, and in complexes  $[\mathbf{2}]^{2+}$ ,  $[\mathbf{3}]^+$ , and **4**, two tetradentate ligands coordinate a single Co(II) center in a tridentate meridional fashion with one uncoordinated azo-arm from each of the ligands. In the presence of reducing agents, the monomers  $[\mathbf{2}]^{2+}$ ,  $[\mathbf{3}]^+$ , and **4** undergo ligand-centered reduction to form azo-anion radicals, and the otherwise pendent azo-arms in the presence of cobalt(II)-salts like  $\text{Co}(\text{ClO}_4)_2$  or  $\text{CoCl}_2$  bind the second Co(II)-ion; further internal electron transfer from the cobalt center to the arylazo backbone produces the binuclear complex **1**. Spectroscopic analysis, DFT studies, and control experiments were performed to understand the electronic structures and the ligand-centered redox-controlled interconversion. The application of complex **1** as a molecular memory device (memristor) was also explored. Complex **1** showed encouraging results as a memristor with a current ON/OFF ratio  $> 10^4$  and is highly promising for resistive RAM/ROM applications.



## INTRODUCTION

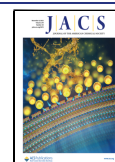
The emergence of various artificial intelligence (AI) related problem-solving protocols such as real-time voice recognition, pattern recognition, image processing, live health monitoring and supporting system, instantaneous decision-making algorithms, and many more has resulted in the need for huge information processing and storage capabilities.<sup>1,2</sup> However, conventional computers are not capable enough due to the "von Neumann bottleneck" issue.<sup>3</sup> Accordingly, the memristor technology has emerged as an attractive alternative for highly efficient computing platforms such as in-memory and neuromorphic computing. Various materials, including organic semiconductors (OSCs),<sup>4</sup> polymers,<sup>5,6</sup> metal oxides,<sup>7–9</sup> quantum dots (QDs),<sup>10</sup> and two-dimensional (2D) transition metal dichalcogenides (TMDs),<sup>11–13</sup> have been explored to develop high-performance memristors. Among these, the oxide-based devices produce the most promising results; however, their applications are restricted because of the high voltage/current and large set/reset voltage. On the other hand, organic semiconductors are attracting considerable interest due to their tunable electronic properties and easy solution

processability. Despite significant efforts, these devices, however, suffer from reproducibility, slow switching speed, stability, endurance, and scalability.

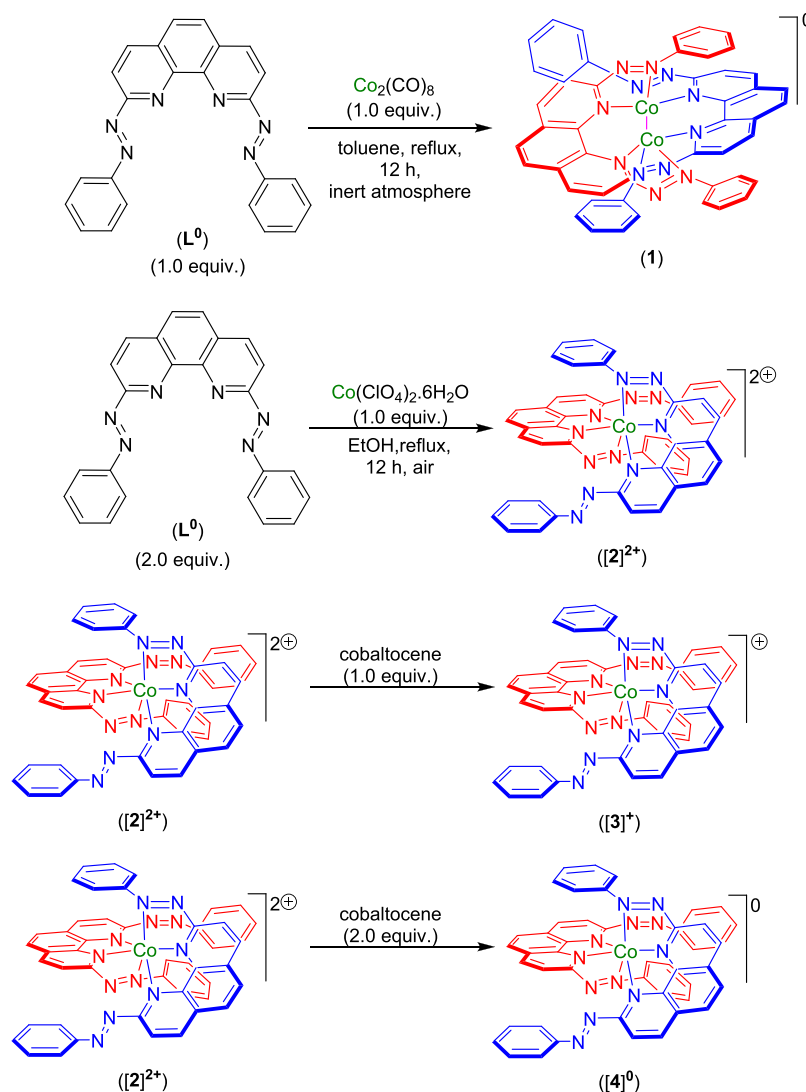
In this regard, coordination complexes containing organic ligands bound with a metal center offer a promising alternative.<sup>14</sup> The extra stability gained by organic compounds (ligands) upon metal-ion coordination may overcome the short lifetime and thermal instability issues of organic semiconductors for various electronic and optoelectronic applications. Moreover, the redox-active nature of the coordinated metal ions adds an extra advantage over the simple organic semiconductors. Furthermore, if both the coordinated organic compound (ligand) and the metal ions are

Received: August 22, 2022

Published: October 25, 2022



Scheme 1. Synthesis of the Cobalt Complexes



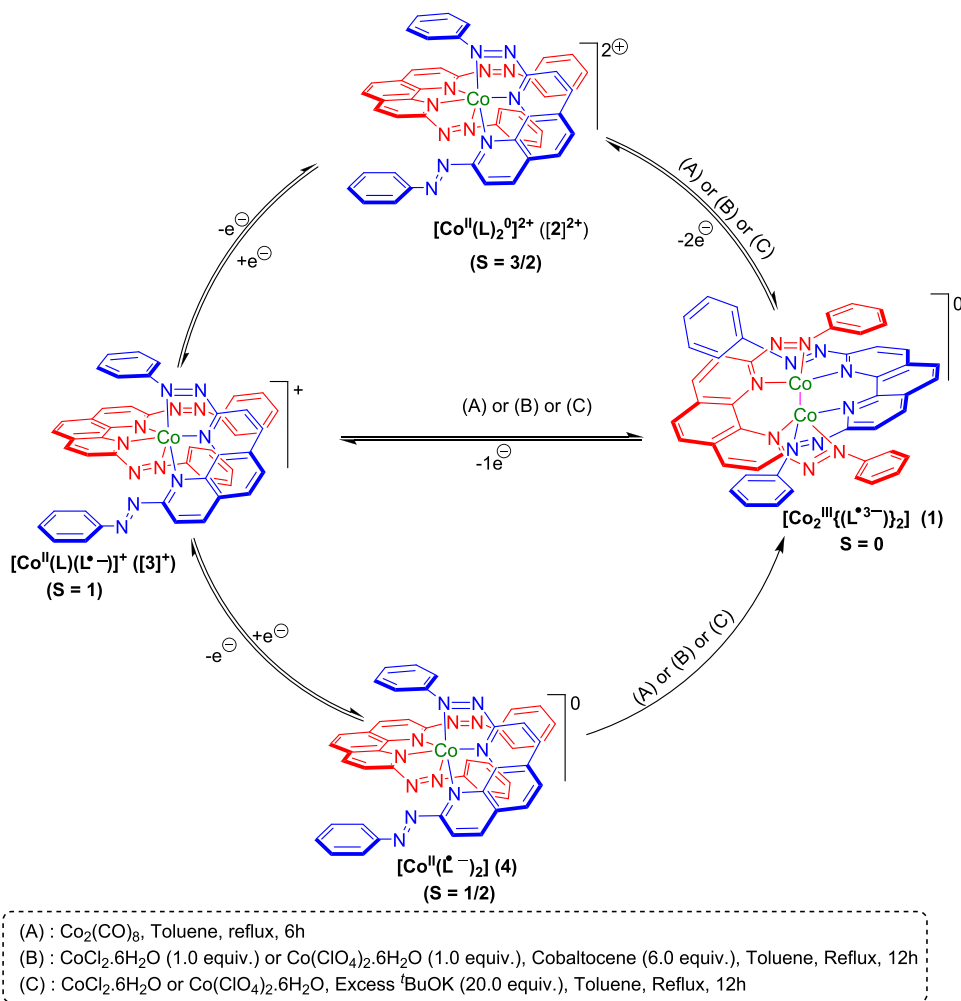
redox-active, the metal and the ligand can cooperate during electron transfer processes.

The chemistry of transition metal complexes of redox-active organic molecules (ligands) is currently undergoing a renaissance because these ligands when coordinated to transition metal ions can play an important role in controlling the overall redox properties of the complexes. Initially, the research in this area was focused on understanding the ambiguous electronic structure description,<sup>15</sup> which later on shifted to catalysis,<sup>16</sup> and very recently, it turned more toward physical applications.<sup>14,17–19</sup> In recent years, this class of complexes has also been used for the fabrication of various semiconductor devices.<sup>14,17–19</sup>

Herein, we report a ligand-centered redox-controlled strategy for the synthesis of an unusual binuclear diradical cobalt(III) complex,  $[Co_2^{III}(L^{\bullet 3-})_2]$  (**1**), featuring two three-electron reduced trianionic monoradical 2,9-bis(phenyldiazo)-1,10-phenanthroline ligands ( $L^{\bullet 3-}$ ) and two intermediate-spin cobalt(III) centers having a Co–Co bond. Controlled ligand-centered oxidation of **1** afforded two mononuclear complexes,  $[Co^{II}(L^{\bullet -})(L^0)]^+$  (**[3]<sup>+</sup>**) and  $[Co^{II}(L^0)_2]^{2+}$  (**[2]<sup>2+</sup>**), which upon further ligand-centered reduction yielded a di-azo-anion diradical complex,  $[Co^{II}(L^{\bullet -})_2]$  (**4**). In complex **1**, two three-

electron reduced di-azo-anion monoradical ligands ( $L^{\bullet 3-}$ ) bridge two intermediate Co(III) centers at a distance of 2.387(2) Å, while upon oxidation, one of the coordinating azo-arms of **L** becomes pendent, and in complexes **[2]<sup>2+</sup>**, **[3]<sup>+</sup>**, and **4**, two tetradentate ligands coordinate a single Co(II) center in a tridentate meridional fashion with one uncoordinated azo-arm from each of the ligands. In the presence of reducing agents, the monomers **[2]<sup>2+</sup>**, **[3]<sup>+</sup>**, and **4** undergo ligand-centered reduction, and the otherwise pendent azo-arms in the presence of cobalt(II)-salts like  $Co(ClO_4)_2$  or  $CoCl_2$  bind the second Co(II)-ion; further internal electron transfer from the cobalt center to the arylazo backbone produces the binuclear complex **1**. Spectroscopic analysis, DFT studies, and control experiments were performed to understand the electronic structures and the facile ligand-centered redox-controlled interconversion between the mononuclear and the binuclear species. Current–voltage ( $I$ – $V$ ) characteristics (in the solid state) were studied to explore the plausible application of **1** and **[2]**( $ClO_4$ )<sub>2</sub> as a molecular data storage device (memristor) through the novel resistive switching phenomenon.

Scheme 2. Redox-Induced Interconversion



## RESULT AND DISCUSSION

**Synthesis, Characterization, and Redox-Induced Interconversion.** The reaction of the neutral ligand 2,9-bis(phenyldiazo)-1,10-phenanthroline ( $\text{L}^0$ ) with  $\text{Co}_2(\text{CO})_8$  under an inert atmosphere in toluene at  $110^\circ\text{C}$  afforded a binuclear reddish-brown color complex,  $[\text{Co}_2^{\text{III}}\{\text{L}^{\bullet 3-}\}_2]$  (**1**), in 72% yield (Scheme 1). On the other hand, the reaction of  $\text{Co}(\text{ClO}_4)_2 \cdot 6\text{H}_2\text{O}$  with  $\text{L}^0$  produces a six-coordinate dicationic mononuclear Co(II) complex,  $[\text{Co}^{\text{II}}(\text{L})_2](\text{ClO}_4)_2$  (**[2]**- $(\text{ClO}_4)_2$ ), in 80% yield (Scheme 1). Complex **[2]** $^{2+}$  upon one-electron reduction with cobaltocene transforms to a monocationic brown-colored monoradical complex,  $[\text{Co}^{\text{II}}(\text{L})(\text{L}^{\bullet -})](\text{ClO}_4)_2$  (**[3]**- $(\text{ClO}_4)_2$ ), while upon two-electron reduction, a diradical species,  $[\text{Co}^{\text{II}}(\text{L}^{\bullet -})_2]$  (**4**), is formed. Complex **4** was also obtained from the stoichiometric reaction of  $\text{Co}_2(\text{CO})_8$  with ( $\text{L}^0$ ) in THF at room temperature. Interestingly, in the presence of reducing agents like cobaltocene or  $\text{KO}^t\text{Bu}$ , the reaction of the preformed monomers **[2]** $^{2+}$ , **[3]** $^+$ , or **4** with  $\text{Co}^{\text{II}}\text{Cl}_2 \cdot 6\text{H}_2\text{O}$  or  $\text{Co}^{\text{II}}(\text{ClO}_4)_2 \cdot 6\text{H}_2\text{O}$  produces the binuclear complex **1** in 46, 55, and 53% yields, respectively, under an inert atmosphere (Scheme 2). In the absence of reducing agents, we did not observe the formation of complex **1**. In the presence of reducing agents, the coordinated arylazo scaffolds undergo three-electron reduction (vide infra), which in turn enhances its coordinating ability and allows the otherwise pendent azo-

chromophores to bind the second cobalt-ion leading to the formation of **1**. The ligand-centered redox-controlled formation of **1** from **[2]** $^{2+}$  is further supported by the fact that the stoichiometric reaction of  $\text{Co}_2(\text{CO})_8$  with the preformed **[2]** $^{2+}$  under an argon atmosphere in toluene at  $110^\circ\text{C}$  afforded the binuclear complex **1** in 42% yield. Notably, the stoichiometric reaction of  $\text{Co}_2(\text{CO})_8$  with **[3]** $^+$  and **4** also afforded the binuclear complex **1** (Scheme 2). On the other hand, the oxidation of **1** using ferrocenium cation produces **[3]** $^+$  and **[2]** $^{2+}$ , respectively.

Elemental analyses support the formulation of these complexes. Complex **1** is diamagnetic and shows  $^1\text{H}$  NMR signals in the 6.47–8.54 ppm range. Complexes **[2]** $^{2+}$ , **[3]** $^+$ , and **4**, on the other hand, are all paramagnetic in nature with room temperature magnetic moment  $\mu_{\text{eff}}$  values of 4.95, 3.79, and  $2.47 \mu\text{B}$ , respectively.

**X-ray Single-Crystal Structure.** The identity of these complexes was confirmed by single-crystal X-ray diffraction studies (Figure 1). The X-ray structure of compound **1** confirms the formation of a binuclear complex (Figure 1a). Two cobalt centers are coordinated by two azo-aromatic ligands **L**. Each ligand is coordinated to the cobalt center in a bidentate fashion using one N-donor atom of the 1,10-phenanthroline moiety and one N-atom of the azo-chromophore; the other N-donor atom of the 1,10-phenanthroline moiety and the second azo-chromophore

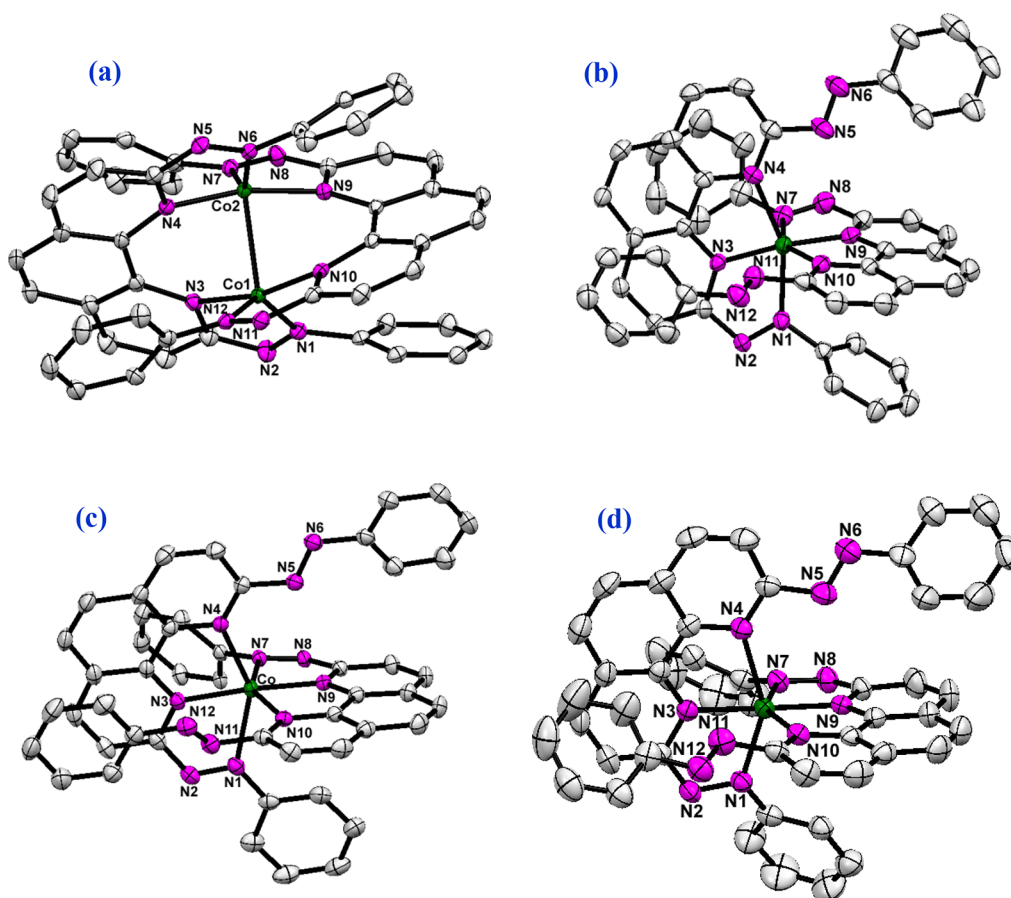


**Figure 1.** ORTEP plots of (a) complex **1**, (b) complex **[2](ClO<sub>4</sub>)<sub>2</sub>**, (c) complex **[3](PF<sub>6</sub>)**, and (d) complex **4** drawn at 50% probability (counter anions and hydrogen atoms are removed for clarity).

coordinate the second cobalt center. Thus, the ligand acts as a bridge between the two cobalt centers. The Co–Co distance of 2.387(2) Å indicates the presence of a cobalt–cobalt bond. The coordination geometry around each cobalt ion is distorted trigonal bipyramidal showing a  $\tau$  value of 0.53 and 0.54, respectively.<sup>20</sup> Complex **[2]**<sup>2+</sup> was crystallized as the perchlorate salt, and its molecular structure consists of one [Co(L)<sub>2</sub>]<sup>2+</sup> cation and two perchlorate anions, leading to the molecular formula [Co<sup>II</sup>(L)<sub>2</sub>](ClO<sub>4</sub>)<sub>2</sub>. Complex **[3]**<sup>+</sup> was crystallized as the PF<sub>6</sub> salt. The molecular structure of **[3](PF<sub>6</sub>)** consists of one [Co(L)<sub>2</sub>]<sup>+</sup> cation and one hexafluorophosphate anion, leading to the molecular formula [Co<sup>II</sup>(L)<sub>2</sub>](PF<sub>6</sub>), while complex **4** is neutral, having only one [Co(L)<sub>2</sub>] unit in its unit cell. Interestingly, in all these three complexes, two tridentate ligands **L** are coordinated to the central Co(II)-ion in a tridentate meridional fashion, yielding a distorted octahedral geometry with one uncoordinated pendent azo-chromophore from each ligand (Figure 1).

The most striking observations in the crystal structures of **1** and **[2]**<sup>2+</sup>, **[3]**<sup>+</sup>, and **4** are the significantly different N=N and Co–N bond lengths. The N=N bond lengths are known to be sensitive to the formal oxidation state of the coordinated arylazo scaffolds and are often used as an indicator of the charge and oxidation state of these ligands in a metal-bound state.<sup>15b</sup> In complex **1**, all the four coordinated N=N bonds were found to be significantly elongated (1.350(1), 1.335(1), 1.343(1), and 1.341(1) Å). Given the diamagnetic nature of **1**, the elongated N=N bond leads to several different limiting electronic structure possibilities: [Co<sub>2</sub><sup>I</sup>(L<sup>•-</sup>)<sub>2</sub>] (*S* = 0),

[Co<sub>2</sub><sup>II</sup>(L<sup>2-</sup>)<sub>2</sub>] (*S* = 0), or [Co<sub>2</sub><sup>III</sup>(L<sup>•3-</sup>)<sub>2</sub>] (*S* = 0). The bond lengths are, in fact, suggestive of the presence of two three-electron reduced ligands L<sup>•3-</sup> (containing net one unpaired electron on each ligand) coordinated to two intermediate spin Co(III) centers with antiferromagnetic coupling between the unpaired electrons (*S* = 0). The distorted trigonal bipyramidal coordination geometry around each of the cobalt centers, along with the elongated N=N distances, points to either cobalt(III) or cobalt(II), but the Co–N distances (Co1–N1, 1.857(2) Å; Co1–N3, 1.919(2) Å; Co2–N4, 1.919(3) Å; Co2–N6, 1.859(2) Å; Co1–N7, 1.858(3) Å; Co1–N9, 1.911(2) Å; Co2–N10, 1.919(3) Å; and Co2–N12, 1.857(3) Å) are most typical for cobalt(III) systems, thus pointing to a [Co<sub>2</sub><sup>III</sup>(L<sup>•3-</sup>)<sub>2</sub>] (*S* = 0) electronic structure.<sup>15</sup> In the IR spectrum of **1**, only one N=N stretching frequency was observed at 1338 cm<sup>-1</sup>, indicating that all the azo-chromophores are identical. Moreover, the significantly lower N=N stretching compared to that of the free azo-chromophores in **L** points to the presence of multiple electrons in the vacant π\* orbital of L<sup>0</sup> as reflected in the significantly elongated N=N bonds in the solid-state X-ray single-crystal data.<sup>15b,16f</sup> XPS analysis and DFT studies were performed to shed light on the ambiguous electronic structure of **1**, which indeed support the [Co<sub>2</sub><sup>III</sup>(L<sup>•3-</sup>)<sub>2</sub>] (*S* = 0) electronic configuration (see below). In complex **[2]**<sup>2+</sup>, the coordinated azo-chromophores are slightly elongated (N=N = 1.269(5) and 1.271(4) Å), whereas the uncoordinated pendent azo-chromophores have N=N distances of 1.244(5) and 1.259(5) Å, respectively. The slight elongation of the

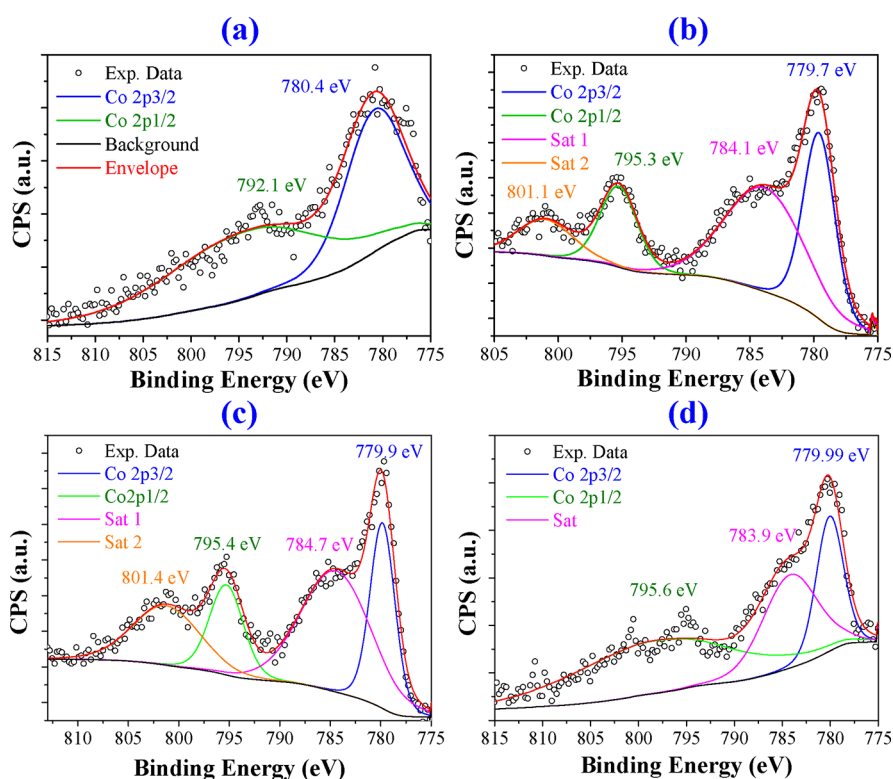


**Figure 2.** XPS spectra of the Co centers of (a) **1**, (b)  $[2](\text{ClO}_4)_2$ , (c)  $[3](\text{PF}_6)$ , and (d) **4**. Experimental data (black open circle bullets), envelope (red), background (black), Co  $2p_{3/2}$  (blue), Co  $2p_{1/2}$  (green), and satellite peaks (magenta and orange).

coordinated azo-chromophores may be attributed to the metal( $d\pi$ )  $\rightarrow$  ligand( $\pi^*$ ) back-donation. In complex  $[3]^+$ , out of the two coordinated azo-chromophores, one  $\text{N}=\text{N}$  bond is sufficiently elongated ( $\text{N}=\text{N} = 1.310(3)$  Å), whereas the other coordinated azo-chromophore has a  $\text{N}=\text{N}$  distance of  $1.270(3)$  Å. The uncoordinated azo-chromophores have  $\text{N}=\text{N}$  distances of  $1.249(3)$  and  $1.261(3)$  Å, respectively. In comparison, in complex **4**, coordinated azo-chromophores are significantly elongated ( $\text{N}=\text{N} = 1.330(5)$  and  $1.330(5)$  Å), and the  $\text{N}=\text{N}$  distances of the pendent azo-chromophores are  $1.249(8)$  Å. These bond length data altogether indicate that in  $[2]^{2+}$ , the coordinated ligands are unreduced ( $\text{L}^0$ ) with the electronic configuration of  $[\text{Co}^{\text{II}}(\text{L})_2]^{2+}$  ( $S = 3/2$ ), while in  $[3]^+$ , one of the coordinated ligand is in one-electron reduced azo-anion radical oxidation state ( $\text{L}^{\bullet-}$ ) with the electronic configuration of  $[\text{Co}^{\text{II}}(\text{L}^{\bullet-})(\text{L})]^+$  ( $S = 1$ ). In complex **4**, both the coordinated ligands are one-electron reduced with the electronic configuration of  $[\text{Co}^{\text{II}}(\text{L}^{\bullet-})_2]$  ( $S = 1/2$ ).

**Cyclic Voltammetry.** Cyclic voltammograms of **1** and  $[2](\text{ClO}_4)_2$  were recorded in  $\text{CH}_3\text{CN}$  solutions containing  $0.1$  M  $[\text{Bu}_4\text{N}]\text{ClO}_4$  at  $25$  °C; potentials are referenced to the saturated  $\text{Ag}/\text{AgCl}$  electrode. The cyclic voltammograms and the results are summarized in the Supporting Information (SI). Complex **1** undergoes two irreversible oxidations at  $0.15$  and  $0.58$  V and one irreversible reduction at  $-1.25$  V. After one or two scans, the color of the solution changes to brown, and the initial voltammogram could not be reproduced. The non-reproducibility of the voltammogram may be attributed to the fact that, upon oxidation, complex **1** transforms to the mononuclear complexes  $[3]^+$  and  $[2]^{2+}$  as observed during chemical oxidation using ferrocenium cation. Complex  $[2]^{2+}$ , on the other hand, exhibited one reversible oxidation at  $0.18$  V and multiple reductions in the potential range of  $-0.2$  to  $-1.5$

V. Molecular orbital analysis reveals that, in complex **1**, both HOMOs and LUMOs are ligand centered, while in complex  $[2]^{2+}$ , HOMO is metal centered and LUMOs are ligand centered. Therefore, the redox responses observed for complex **1** all seem to be ligand centered, while for complex  $[2]^{2+}$ , the oxidation seems to involve the  $\text{Co}(\text{II})/\text{Co}(\text{III})$  redox couple and the reductions are ligand centered. Ligand-centered reductions are further supported by the X-ray single-crystal structural data and redox-induced interconversion (see above).

**XPS Analysis.** XPS analysis was performed on polycrystalline samples of complex **1** and compared with the XPS spectrum of the well-defined  $\text{Co}(\text{II})$  complexes  $[2](\text{ClO}_4)_2$ ,  $[3]\text{PF}_6$ , and **4** to get information about the oxidation state of the two Co centers present in complex **1** (Figure 2). Complex  $[2](\text{ClO}_4)_2$ ,  $[3]\text{PF}_6$ , and **4** showed typical high-spin  $\text{Co}(\text{II})$  type XPS spectra with a  $\text{Co } 2p_{3/2}$  peak at  $779.7$ ,  $779.9$ , and  $779.99$  eV and an intense and well-resolved satellite peak at  $784.1$ ,  $784.7$ , and  $783.9$  eV, respectively.<sup>21</sup> A significantly different XPS spectrum was observed for complex **1**. Complex **1** showed a typical low-spin  $\text{Co}(\text{III})$  type XPS spectrum with a prominent peak for the  $\text{Co } 2p_{3/2}$  state at  $780.4$  eV and no satellite peak in the  $785$  eV region, as expected for high/low-spin  $\text{Co}(\text{II})$  systems. Notably,  $\text{Co}(\text{III})$  systems usually exhibit a prominent main peak in the  $\text{Co } 2p_{3/2}$  region with a little evidence of the satellite peak at the high binding energy side of this peak, while low-spin  $\text{Co}(\text{II})$  systems show, along with the prominent  $2p_{3/2}$  peak, a less intense and less well-resolved satellite peak compared to that observed for high-spin  $\text{Co}(\text{II})$  systems. Therefore, from these experimental evidences, complexes  $[2]^{2+}$ ,  $[3]^+$ , and **4** seem to have a high-spin  $\text{Co}(\text{II})$  electronic configuration, while in complex **1**, the two cobalt centers possess an intermediate-spin  $\text{Co}(\text{III})$  electronic configuration. The X-ray single-crystal structure data, room

temperature magnetic data, and DFT studies are in agreement with an intermediate-spin Co(III) electronic structure description in **1**.

**DFT Studies.** To elucidate the electronic structure of **1**, a broken-symmetry (BS) hybrid density functional theory (DFT) calculation was conducted at the B3LYP level.<sup>22</sup> The electronic structure of compound **1** is complex. The DFT optimized geometries (B3LYP, def2-TZVP) computed at the  $S = 1$ ,  $S = 2$ , and broken symmetry<sup>23</sup>  $S = 0$  spin states are pretty close in energy (Table 1). In agreement with the

**Table 1. Relative SCF Energies of Complex 1 Optimized in Different Spin States (b3-lyp, def2-TZVP, disp3)**

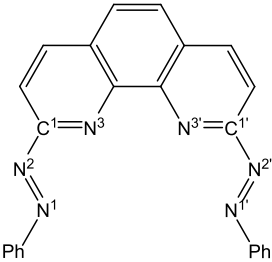
spin state	$\langle S^2 \rangle$	unpaired electrons	rel. energy (kcal mol <sup>-1</sup> )
$S = 0$ , closed shell	0	0	= 0
$S = 0$ , broken symm.	3.3474	0	-13.1 (spin corrected) (uncorrected: -8.5)
$S = 1$	4.3741	2	-11.6
$S = 2$	7.4724	4	-11.9
$S = 3$	12.1924	6	+7.0
$S = 4$	20.1404	8	+4.7

experimentally determined diamagnetic ground state of complex **1**, the broken symmetry  $S = 0$  singlet solution is computed to be the lowest in energy when correcting for spin contamination.

Comparison of the intraligand bond distances between the DFT optimized structure of  $L_2Co_2$  (**1**) and the optimized structures of the ligand  $L^0$  and its one-, two-, and three-electron reduced forms  $L^-$ ,  $L^{2-}$ , and  $L^{3-}$  reveals that the binuclear complex  $L_2Co_2$  (in the  $S = 0$ , open-shell singlet ground state) contains two  $L^{3-}$  ligands (Table 2). This implies that each cobalt center must have a Co<sup>III</sup> oxidation state.

The spin density plot of complex **1** reveals the presence of an  $\alpha$  spin on each of the cobalt centers and a delocalized  $\beta$  spin on each of the ligands antiferromagnetically coupled to the cobalt spins (Figure 3). Unrestricted corresponding orbital analysis of the broken symmetry  $S = 0$  solution of **1** confirms

**Table 2. Selected Ligand Bond Distances of the Free Ligand L in Four Different Oxidation States ( $L^0$ ,  $L^-$ ,  $L^{2-}$ , and  $L^{3-}$ ) and in Complex  $L_2Co_2$**



	N1–N2/N1'–N2'	N2–C1/N2'–C1'	C1–N3/C1'–N3'
$L^0$ ( $S = 0$ )	1.245	1.422	1.315
$L^{*-}$ ( $S = 1/2$ )	1.275	1.386	1.335
$L^{2-}$ ( $S = 1$ )	1.312	1.369	1.344
$L^{*3-}$ ( $S = 1/2$ )	1.337	1.348	1.365
<b>1</b> ( $L_2Co_2$ , $S = 0$ , BS)	1.320	1.341	1.358
<b>1</b> ( $L_2Co_2$ , X-ray structure)	1.346	1.351	1.361

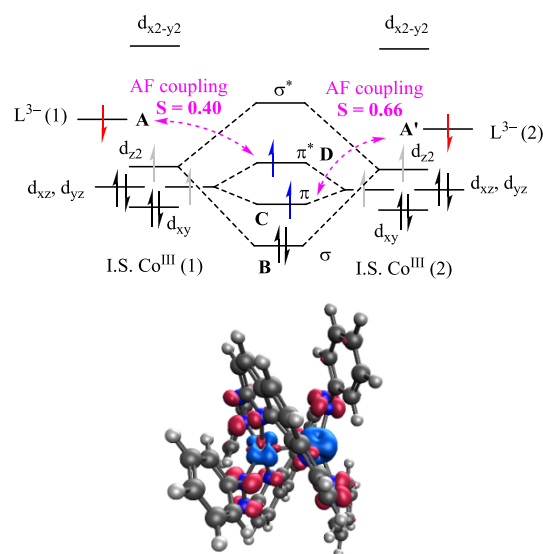


**Figure 3.** Simplified representation of the computed electronic structure (top) and spin density plot (bottom) of complex **1** (broken symmetry  $S = 0$  solution).

the presence of a total of four unpaired electrons, one on each cobalt atom and one on each ligand  $L^{3-}$ . The latter is in agreement with the  $S = 1/2$  spin state of the free tris-anionic ligand  $L^{3-}$  (orbitals A and A'; Figure 4). The presence of one unpaired electron on each cobalt(III) center is a result of a bonding interaction between the two half-filled  $d_{z^2}$  orbitals of the intermediate-spin cobalt(III) centers in the distorted coordination geometry of **1** leading to a doubly occupied  $\sigma$ -bond between the two cobalt(III) atoms (orbital B in Figures 3

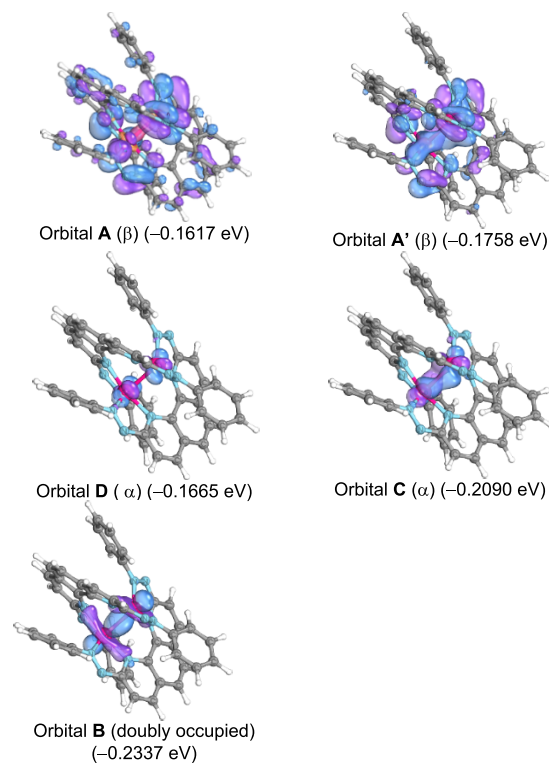


**Figure 4.** Selected UCO orbitals in **1** (labels chosen as shown in Figure 3).

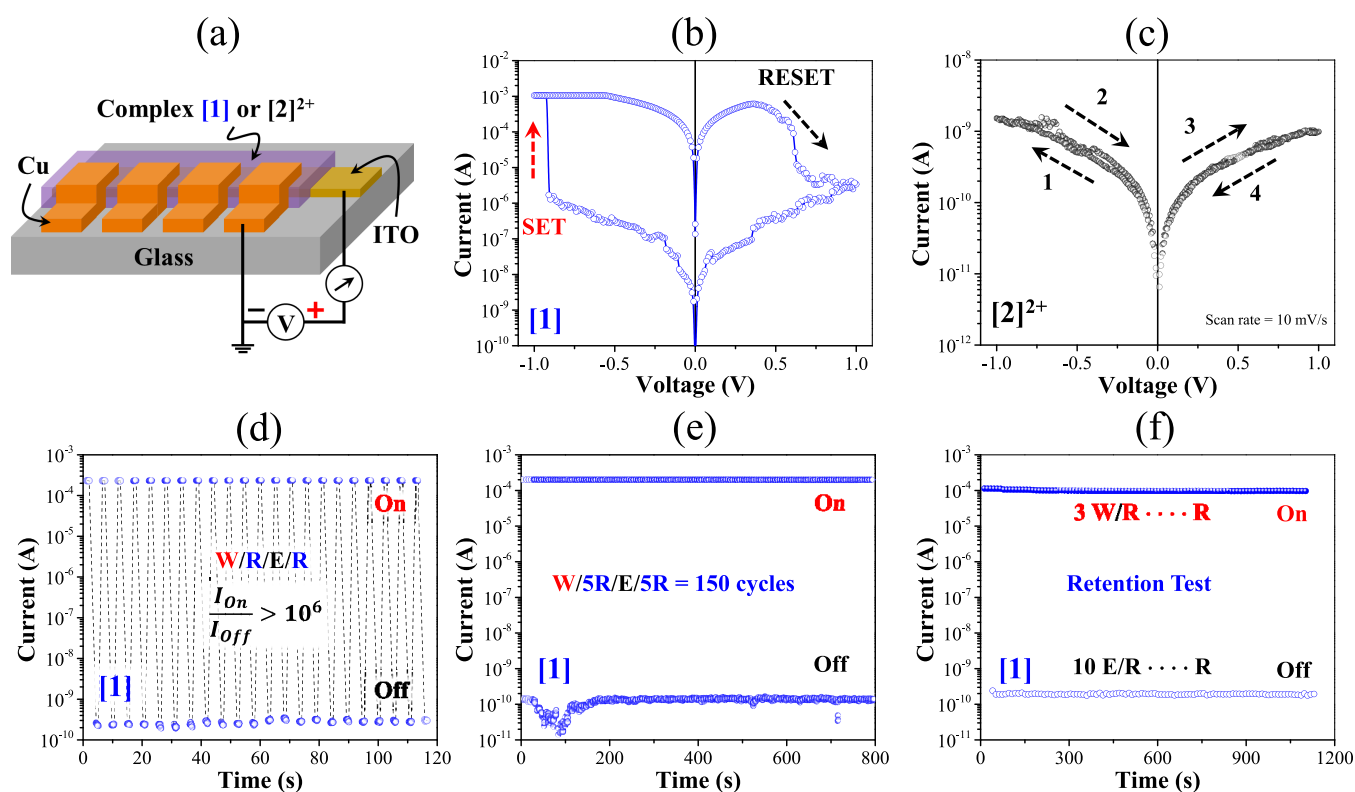


**Figure 5.** (a) Memristor thin film device architecture ITO/sample/Cu shown schematically. (b, c) Current–voltage ( $I$ – $V$ ) characteristics of complex 1 and  $[2](\text{ClO}_4)_2$  recorded in a loop. Arrows indicate the sweep direction. (d) Write/read/erase/read (W/R/E/R) cycles of the complex 1 device for ReRAM application. (e) Endurance test for 150 W/R/E/R cycles. (f) Retention test for both the ON (filled circle) and OFF (open circle) states by applying 2 and 10 consecutive W and E pulses, respectively, before starting reading.

and 4). The remaining half-filled  $d_{xz}/d_{yz}$  orbitals on both cobalt centers interact via weak  $\pi$ -bonding (orbital C) and  $\pi^*$  antibonding interactions (orbital D) with a small orbital splitting between them, leaving both orbitals half-filled with a single  $\alpha$ -electron. The two half-filled ligand-centered orbitals A and A' each contain a  $\beta$ -electron, which is antiferromagnetically coupled to the two cobalt-centered  $\alpha$ -electrons in orbitals D and C, respectively (net DFT calculated AF coupling constant:  $J = -1344.82 \text{ cm}^{-1}$ ) (Figures 3 and 4).

While this representation is in agreement with the experimental data, the "real" electronic structure of **1** is undoubtedly more complex, and likely, multiple electronic states contribute to the ground state of this unusual molecule. A more accurate description of the unusual electronic ground state of complex **1** would require the use of a multireference (post-HF) method such as CASSCF-NEVPT2, but such calculations are currently out of reach considering the large active space required for this molecule. Geometry optimization of complex  $[2]^{2+}$  reveals that a high-spin Co(II)-ion ( $S = 3/2$ ) is coordinated to two unreduced azo-aromatic ligands  $\text{L}^0$ . Spin density analysis shows that the Co(II) center possesses +2.687 ( $\alpha$  spin). Complex  $[3]^+$  was found to be an open-shell triplet ( $S = 1$ ). Broken symmetry density functional calculations reveal that a high-spin Co<sup>II</sup> center is coordinated to a one-electron reduced open-shell  $\pi$ -radical monoanion ( $\text{L}^{\bullet-}$ ) and neutral ligand  $\text{L}^0$ . Spin density calculation shows that the metal center contains +2.76 spin populations and that each of the ligand centers has its respective spin of  $-0.277$  and  $-0.231$ , mainly localized on the azo-chromophore, revealing the higher degree of metal–ligand delocalization. This suggests that the electronic structure of  $[3]^+$  is best described as  $[\text{Co}^{\text{II}}(\text{L}^{\bullet-})$

( $\text{L}^0$ )]<sup>+</sup>. Antiferromagnetic coupling of one ligand-centered spin with the high-spin Co(II) center gives rise to the experimentally observed  $S = 1$  ground state as observed from X-ray single-crystal data and XPS analysis. Complex **4** is found to be a diradical species with a  $[\text{Co}^{\text{II}}(\text{L}^{\bullet-})_2]$  electronic structure. Broken symmetry calculations reveal that a high-spin Co(II) ion is coordinated to two one-electron reduced azo-anion radical ligands ( $\text{L}^{\bullet-}$ ). Spin density analysis reveals that the cobalt center possesses +2.751 ( $\alpha$ ) spin population and that each of the coordinated ligands **L** possesses  $-0.836$  ( $\beta$ ) spin population, particularly localized on the azo-chromophore.

**Memristor Property.** With the above results in hand, next we explored the resistive switching (RS) property of **1** and  $[2](\text{ClO}_4)_2$  as a memristor and in related applications. Accordingly, thin film devices were fabricated as a sandwiched layer of thickness about 660 nm in between two orthogonal electrodes, ITO and copper (Cu), as illustrated in Figure 5a. The current–voltage ( $I$ – $V$ ) characteristics in a loop were recorded for both the devices of **1** and  $[2]^{2+}$  by sweeping bias voltage starting from 0 to +1.0 to  $-1.0$  V and back to 0 V again in step of 10 mV at NPLC 1 as illustrated in Figure 5b,c. Interestingly, a robust nonvolatile RS is observed for **1** with a current ON/OFF ratio  $> 10^4$ , which remains absent for  $[2]^{2+}$  and ( $\text{L}^0$ ) (see SI Figure S12). This observed conductivity jump from a low (OFF) to a high (ON) state is an exciting feature for molecular memristor devices.<sup>10</sup> Our present work represents a remarkable achievement toward the requirement of desired metrics for nonvolatile RS-based molecular memristor devices.<sup>11</sup> The robustness of our molecular memristor device is further emphasized by testing for resistive

random access memory (ReRAM) application in the form of endurance and retention. In a control test, the RS property of the thin film device fabricated using the free ligand  $L^0$  was also investigated using similar parameters, which shows only the semiconducting nature without the signature of any RS (see SI). Hence, it is strongly evident that complex **1** is a promising material for the further development of memristors with the desired metrics and related applications. The exact mechanism for the promising RS property of **1** is not completely clear to us, and it requires further studies. However, literature reports on RS properties of a few similar azo-based transition metal complexes indicate that the ligand-centered redox events in **1** play a key role in the observed resistive switching of **1**.<sup>18,19</sup>

The promising and consistent RS behavior of the device fabricated from **1** prompted us to do the testing for memristor-based data storage application. Figure 5d shows the ReRAM application of the device based on **1** for 22 W/R/E/R cycles in which a write (W) voltage pulse of  $-1$  V for 1 s was applied followed by five read (R) pulses of  $-0.1$  V for 0.1 s and then an erase (E) pulse of  $+1$  V for 2 s followed by five read (R) pulses as earlier for a "W/R/E/R" cycle. This result confirms the highly reversible nature of our molecular memory device between the ON and OFF conducting states. Resembling the opulent  $I$ - $V$  characteristic of RS property, a distinct and stable nature for both the ON and OFF states is observed. Endurance and retention are two very important parameters for a nonvolatile RS device, and those are recorded for the RS device based on **1** as shown in Figure 5e,f. The endurance test for 150 "W/R/E/R" cycles (Figure 5e) clearly shows a stable and distinct switching between the ON and OFF conducting states. Then, we probed the retention of both the ON and OFF states as depicted in Figure 5f, which is recorded for more than 1000 s by repeating the read pulses of  $+0.2$  V for 0.1 s at an interval of 1 s after applying three consecutive W pulses of  $-1$  V for 3 s with 1 s intervals to induce the ON state and 10 consecutive E pulses of  $+1$  V for 2 s with 1 s intervals to return back to the OFF state. Our device using complex **1** shows a fairly stable retention of states without any trace of conductivity fluctuation, which is highly desirable as a potential candidate in the existing library of molecular materials for robust memristor application.

## CONCLUSIONS

In conclusion, we have reported a ligand-centered redox-controlled strategy for the synthesis of an unusual binuclear singlet-diradical cobalt(III) complex,  $[\text{Co}_2^{\text{III}}(\text{L}^{\bullet 3-})_2]$  (**1**), featuring two three-electron reduced tetradentate di-azo-anion diradical ligands. Upon controlled ligand-centered oxidation, the dimeric complex **1** transforms to the mononuclear species  $[3]^+$  and  $[2]^{2+}$ , which upon ligand-centered reductions produce the mononuclear diradical species **4**. The monomers  $[2]^{2+}$ ,  $[3]^+$ , and **4** in the presence of reducing agents undergo facile ligand-centered reduction to form azo-anion radicals, and the otherwise pendent azo-arm in the presence of cobalt(II)-salts like  $\text{Co}(\text{ClO}_4)_2$  or  $\text{CoCl}_2$  binds the second Co(II)-ion; further internal electron transfer from the cobalt center to the arylazo backbone produces the dimer **1**. The diradical complex **1** exhibits a pinched hysteresis loop in the  $I$ - $V$  curve featuring its superior RS property for memristor and related data storage applications. The device is suitable for ReRAM application with a current ON/OFF ratio  $> 10^6$  at a low operating voltage. We believe that complex **1** has the potential to show excellent nonvolatile resistive switching

properties and will become a promising material for thin film memristors and related applications in the near future, including neuromorphic computations<sup>24</sup> and broadly the field of artificial intelligence (AI) as an energy-efficient alternative. Our studies in this area are ongoing and will be reported in due course.

## ASSOCIATED CONTENT

### Supporting Information

The Supporting Information is available free of charge at <https://pubs.acs.org/doi/10.1021/jacs.2c08941>.

Experimental procedure, ORTEP diagrams, crystal data and structure refinement parameters, selected crystallographic bond lengths,  $^1\text{H}$  NMR spectrum of complex **1**, UV-vis absorption spectra (in solution and solid state (thin film)), cyclic voltammogram, spin density plots, thin-film thickness from profilometer line profile, current-voltage ( $I$ - $V$ ) characteristics of the ligand ( $L^0$ ) molecule based device ITO/ $(L^0)$ /Cu, optimized coordinates, and references (PDF)

Optimized geometries (ZIP)

### Accession Codes

CCDC 2144561–2144562 and 2202810–2202811 contain the supplementary crystallographic data for this paper. These data can be obtained free of charge via [www.ccdc.cam.ac.uk/data\\_request/cif](http://www.ccdc.cam.ac.uk/data_request/cif), or by emailing [data\\_request@ccdc.cam.ac.uk](mailto:data_request@ccdc.cam.ac.uk), or by contacting The Cambridge Crystallographic Data Centre, 12 Union Road, Cambridge CB2 1EZ, UK; fax: +44 1223 336033.

## AUTHOR INFORMATION

### Corresponding Authors

**Bikas C. Das** – Emerging Nanoelectronic Devices Research Laboratory (eNDR Lab), School of Physics, Indian Institute of Science Education and Research Thiruvananthapuram (IISER TVM), Thiruvananthapuram 695551 Kerala, India; [orcid.org/0000-0002-4750-0542](https://orcid.org/0000-0002-4750-0542); Email: [bikas@iisertvm.ac.in](mailto:bikas@iisertvm.ac.in)

**Nanda D. Paul** – Department of Chemistry, Indian Institute of Engineering Science and Technology, Shibpur, Howrah 711103, India; [orcid.org/0000-0002-8872-1413](https://orcid.org/0000-0002-8872-1413); Email: [ndpaul2014@chem.iists.ac.in](mailto:ndpaul2014@chem.iists.ac.in), [ndpaul@gmail.com](mailto:ndpaul@gmail.com)

### Authors

**Suman Sinha** – Department of Chemistry, Indian Institute of Engineering Science and Technology, Shibpur, Howrah 711103, India

**Muhammed Sahad E** – Emerging Nanoelectronic Devices Research Laboratory (eNDR Lab), School of Physics, Indian Institute of Science Education and Research Thiruvananthapuram (IISER TVM), Thiruvananthapuram 695551 Kerala, India

**Rakesh Mondal** – Department of Chemistry, Indian Institute of Engineering Science and Technology, Shibpur, Howrah 711103, India; [orcid.org/0000-0003-2564-733X](https://orcid.org/0000-0003-2564-733X)

**Siuli Das** – Department of Chemistry, Indian Institute of Engineering Science and Technology, Shibpur, Howrah 711103, India

**Litty Thomas Manamel** – Emerging Nanoelectronic Devices Research Laboratory (eNDR Lab), School of Physics, Indian Institute of Science Education and Research



Thiruvananthapuram (IISER TVM), Thiruvananthapuram 695551 Kerala, India

Paula Brandão – Departamento de Química/CICECO, Instituto de Materiais de Aveiro, Universidade de Aveiro, 3810-193 Aveiro, Portugal

Bas de Bruin – Homogeneous, Supramolecular and Bio-Inspired Catalysis (HomKat) van't Hoff Institute for Molecular Sciences (HIMS), University of Amsterdam, 1098 XH Amsterdam, The Netherlands; [orcid.org/0000-0002-3482-7669](https://orcid.org/0000-0002-3482-7669)

Complete contact information is available at: <https://pubs.acs.org/10.1021/jacs.2c08941>

### Author Contributions

#S.S., M.S.E., and R.M. contributed equally to this work.

### Notes

The authors declare no competing financial interest.

## ACKNOWLEDGMENTS

The research was supported by DST-SERB, Govt. of India (grant to NDP; Project: CRG/2019/001737). B.C.D. acknowledges the financial support from DST-SERB, Govt. of India (grants CRG/2021/000567 and EEQ/2021/000810). S.S. thanks the IESTS, S.D. and M.S.E. thank the UGC, and R.M. thanks the CSIR for fellowship support. Financial assistance from the IEST, Shibpur, and IISER Thiruvananthapuram is duly acknowledged. We sincerely thank Dr. Subrata Kundu, IISER Thiruvananthapuram, for allowing us to use his laboratory for a few synthetic works. We thank Dr. Serhiy Demeshko and Prof. Dr. Franc Meyer for helpful discussion.

## REFERENCES

- (1) Yuan, J.; Liu, S. E.; Shylendra, A.; Rojas, W. A. G.; Guo, S.; Bergeron, H.; Li, S.; Lee, H.-S.; Nasrin, S.; Sangwan, V. K.; Trivedi, A. R.; Hersam, M. C. Reconfigurable MoS<sub>2</sub> Memristors for Continuous Learning in Spiking Neural Networks. *Nano Lett.* **2021**, *21*, 6432–6440.
- (2) Davenport, T.; Kalakota, R. The Potential for Artificial Intelligence in Healthcare. *Future Healthc J.* **2019**, *6*, 94–98.
- (3) Yuan, L.; Liu, S. Z.; Chen, W. L.; Fan, F.; Liu, G. Organic Memory and Memristors: From Mechanisms, Materials to Devices. *Adv. Electron. Mater.* **2021**, *7*, 2100432.
- (4) (a) Li, C. Y.; Li, D.; Zhang, W. F.; Li, H.; Yu, G. Towards High-Performance Resistive Switching Behavior through Embedding a D-A System into 2D Imine-Linked Covalent Organic Frameworks. *Angew. Chem., Int. Ed.* **2021**, *60*, 27135–27143. (b) Kim, J.; Ohtsu, H.; Den, T.; Deekamwong, K.; Muneta, I.; Kawano, M. Control of Anisotropy of A Redox-Active Molecule Based Film Leads to Non-volatile Resistive Switching Memory. *Chem. Sci.* **2019**, *10*, 10888–10893.
- (5) Das, B. C.; Pillai, R. G.; Wu, Y. L.; McCreery, R. L. Redox-Gated Three-Terminal Organic Memory Devices: Effect of Composition and Environment on Performance. *ACS Appl. Mater. Interfaces* **2013**, *5*, 11052–11058.
- (6) Li, Y.; Qian, Q.; Zhu, X.; Li, Y.; Zhang, M.; Li, J.; Ma, C.; Li, H.; Lu, J.; Zhang, Q. Recent Advances in Organic-based Materials for Resistive Memory Applications. *InfoMat* **2020**, *2*, 995–1033.
- (7) Strukov, D. B.; Snider, G. S.; Stewart, D. R.; Williams, R. S. The Missing Memristor Found. *Nature* **2008**, *453*, 80–83.
- (8) Wedig, A.; Luebben, M.; Cho, D. Y.; Moors, M.; Skaja, K.; Rana, V.; Hasegawa, T.; Adepalli, K. K.; Yildiz, B.; Waser, R.; Valov, I. Nanoscale Cation Motion in TaO<sub>x</sub>, HfO<sub>x</sub> and TiO<sub>x</sub> Memristive Systems. *Nat. Nanotechnol.* **2016**, *11*, 67–74.
- (9) Lee, M.-J.; Lee, C. B.; Lee, D.; Lee, S. R.; Chang, M.; Hur, J. H.; Kim, Y.-B.; Kim, C.-J.; Seo, D.-H.; Seo, S.; Chung, U.-I.; Yoo, I.-K.; Kim, K. A Fast, High-endurance and Scalable Non-volatile Memory Device Made from Asymmetric Ta<sub>2</sub>O<sub>5-x</sub>/TaO<sub>2-x</sub> Bilayer Structures. *Nat. Mater.* **2011**, *10*, 625–630.
- (10) Das, B. C.; Pal, A. J. Switching between Different Conformers of a Molecule: Multilevel Memory Elements. *Org. Electron.* **2008**, *9*, 39–44.
- (11) (a) Sagar, S.; Mohanan, K. U.; Cho, S.; Majewski, L. A.; Das, B. C. Emulation of Synaptic Functions with Low Voltage Organic Memristor for Hardware Oriented Neuromorphic Computing. *Sci. Rep.* **2022**, *12*, 3808. (b) Mukherjee, A.; Sagar, S.; Parveen, S.; Das, B. C. Superionic Rubidium Silver Iodide Gated Low Voltage Synaptic Transistor. *Appl. Phys. Lett.* **2021**, *119*, 253502.
- (12) Ge, R.; Wu, X.; Liang, L.; Hus, S. M.; Gu, Y.; Okogbue, E.; Chou, H.; Shi, J.; Zhang, Y.; Banerjee, S. K.; Jung, Y.; Lee, J. C.; Akinwande, D. A Library of Atomically Thin 2D Materials Featuring the Conductive-Point Resistive Switching Phenomenon. *Adv. Mater.* **2021**, *33*, 2007792.
- (13) Chiang, C. C.; Ostwal, V.; Wu, P.; Pang, C. S.; Zhang, F.; Chen, Z. H.; Appenzeller, J. Memory Applications from 2D Materials. *Appl. Phys. Rev.* **2021**, *8*, No. 021306.
- (14) Goswami, S.; Deb, D.; Tempez, A.; Chaigneau, M.; Rath, S. P.; Lal, M.; Ariando; Williams, R. S.; Goswami, S.; Venkatesan, T. Nanometer-Scale Uniform Conductance Switching in Molecular Memristors. *Adv. Mater.* **2020**, *32*, 2004370.
- (15) (a) Wang, M.; England, J.; Weyhermüller, T.; Kokatam, S.; Pollock, C. J.; DeBeer, S.; Shen, J.; Yap, G. P. A.; Theopold, K. H.; Wieghardt, K. New Complexes of Chromium(III) Containing Organic  $\pi$ -Radical Ligands: An Experimental and Density Functional Theory Study. *Inorg. Chem.* **2013**, *52*, 4472–4487. (b) Ghosh, P.; Samanta, S.; Roy, S. K.; Joy, S.; Krämer, T.; McGrady, J. E.; Goswami, S. Redox Noninnocence in Coordinated 2-(Arylazo)pyridines: Steric Control of Ligand-Based Redox Processes in Cobalt Complexes. *Inorg. Chem.* **2013**, *52*, 14040–14049. (c) Sarkar, B.; Patra, S.; Fiedler, J.; Sunoj, R. B.; Janardanan, D.; Lahiri, G. K.; Kaim, W. Mixed-Valent Metals Bridged by a Radical Ligand: Fact or Fiction Based on Structure-Oxidation State Correlations. *J. Am. Chem. Soc.* **2008**, *130*, 3532–3542. (d) Das, S.; Sinha, S.; Jash, U.; Sikari, R.; Saha, A.; Barman, S. K.; Brandão, P.; Paul, N. D. Redox-Induced Interconversion and Ligand-Centered Hemilability in Ni<sup>II</sup> Complexes of Redox-Noninnocent Azo-Aromatic Pincers. *Inorg. Chem.* **2018**, *57*, 5830–5841.
- (16) (a) Lyaskovskyy, V.; de Bruin, B. Redox Non-Innocent Ligands: Versatile New Tools to Control Catalytic Reactions. *ACS Catal.* **2012**, *2*, 270–279. (b) Mondal, R.; Guin, A. K.; Chakraborty, G.; Paul, N. D. Metal–Ligand Cooperative Approaches in Homogeneous Catalysis using Transition Metal Complex Catalysts of Redox Noninnocent Ligands. *Org. Biomol. Chem.* **2022**, *20*, 296–328. (c) Chirik, P. J. Forum on Redox-Active Ligands. *Inorg. Chem.* **2011**, *50*, 9737–9740. (d) Chirik, P. J.; Wieghardt, K. Radical Ligands Confer Nobility on Base-Metal Catalysts. *Science* **2010**, *327*, 794–795. (e) Broere, D. J. L.; Plessius, R.; van der Vlugt, J. I. New Avenues for Ligand-Mediated Processes – Expanding Metal Reactivity by the Use of Redox-Active Catechol, o-Aminophenol and o-Phenylenediamine Ligands. *Chem. Soc. Rev.* **2015**, *44*, 6886–6915. (f) Das, S.; Mondal, R.; Chakraborty, G.; Guin, A. K.; Das, A.; Paul, N. D. Zinc Stabilized Azo-anion Radical in Dehydrogenative Synthesis of N-Heterocycles. An Exclusively Ligand Centered Redox Controlled Approach. *ACS Catal.* **2021**, *11*, 7498–7512. (g) Sikari, R.; Sinha, S.; Chakraborty, G.; Das, S.; van Leest, N. P.; Paul, N. D. C–N Cross-Coupling Reactions Under Mild Conditions Using Singlet Di-Radical Nickel(II)-Complexes as Catalyst: N-Arylation and Quinazoline Synthesis. *Adv. Synth. Catal.* **2019**, *361*, 4342–4353.
- (17) Liu, J.; Zhou, W.; Liu, J.; Howard, I.; Kilibarda, G.; Schlabach, S.; Coupry, D.; Addicoat, M.; Yoneda, S.; Tsutsui, Y.; Sakurai, T.; Seki, S.; Wang, Z.; Lindemann, P.; Redel, E.; Heine, T.; Wöll, C. Photoinduced Charge-Carrier Generation in Epitaxial MOF Thin Films: High Efficiency as a Result of an Indirect Electronic Band Gap? *Angew. Chem., Int. Ed.* **2015**, *54*, 7441–7445.

(18) Bandyopadhyay, A.; Sahu, S.; Higuchi, M. Tuning of Nonvolatile Bipolar Memristive Switching in Co(III) Polymer with an Extended Azo Aromatic Ligand. *J. Am. Chem. Soc.* **2011**, *133*, 1168–1171.

(19) (a) Goswami, S.; Matula, J. A.; Rath, S. P.; Hedström, S.; Saha, S.; Annamalai, M.; Sengupta, D.; Patra, A.; Ghosh, S.; Jani, H.; Sarkar, S.; Motapothula, M. R.; Nijhuis, C. A.; Martin, J.; Goswami, S.; Batista, V. S.; Venkatesan, T. Robust Resistive Memory Devices Using Solution-Processable Metal-Coordinated Azo Aromatics. *Nat. Mater.* **2017**, *16*, 1262–1270. (b) Paul, N. D.; Rana, U.; Goswami, S.; Mondal, T. K.; Goswami, S. Azo Anion Radical Complex of Rhodium as a Molecular Memory Switching Device: Isolation, Characterization, and Evaluation of Current–Voltage Characteristics. *J. Am. Chem. Soc.* **2012**, *134*, 6520–6523. (c) Seo, K.; Konchenko, A. V.; Lee, J.; Bang, G. S.; Lee, H. Molecular Conductance Switch-On of Single Ruthenium Complex Molecules. *J. Am. Chem. Soc.* **2008**, *130*, 2553–2559.

(20) Addison, A. W.; Rao, T. N.; Reedijk, van Rijn, J. J.; Verschoor, G. C. Synthesis, Structure, and Spectroscopic Properties of Copper(II) Compounds Containing Nitrogen–Sulphur Donor Ligands; The Crystal and Molecular Structure of Aqua[1,7-bis(N-methylbenzimidazol-2'-yl)-2,6-dithiaheptane]copper(II) perchlorate. *Dalton Trans.* **1984**, 1349–1356.

(21) (a) Waldie, K. M.; Ramakrishnan, S.; Kim, S.-K.; Maclaren, J. K.; Chidsey, C. E. D.; Waymouth, R. M. Multielectron Transfer at Cobalt: Influence of the Phenylazopyridine Ligand. *J. Am. Chem. Soc.* **2017**, *139*, 4540–4550. (b) Frost, D. C.; McDowell, C. A.; Woolsey, I. *S. Chem. Phys. Lett.* **1972**, *17*, 320–323.

(22) (a) Becke, A. D.; Thermochemistry, D.-F. III. The Role of Exact Exchange. *J. Chem. Phys.* **1993**, *98*, 5648–5652. (b) Lee, C.; Yang, W.; Parr, R. G. Development of the Colle-Salvetti Correlation-Energy Formula into A Functional of the Electron Density. *Phys. Rev. B: Condens. Matter Mater. Phys.* **1988**, *37*, 785–789.

(23) Noodleman, L.; Case, D. A.; Aizman, A. Broken Symmetry Analysis of Spin Coupling in Iron-Sulfur Clusters. *J. Am. Chem. Soc.* **1988**, *110*, 1001–1005. (b) Noodleman, L.; Davidson, E. R. Ligand Spin Polarization and Antiferromagnetic Coupling in Transition Metal Dimers. *Chem. Phys.* **1986**, *109*, 131–143. (c) Noodleman, L. Valence Bond Description of Antiferromagnetic Coupling in Transition Metal Dimers. *J. Chem. Phys.* **1981**, *74*, 5737–5743.

(24) van de Burgt, Y.; Melianas, A.; Keene, S. T.; Malliaras, G.; Salleo, A. Organic Electronics for Neuromorphic Computing. *Nat. Electron.* **2018**, *1*, 386–397.

## Recommended by ACS

### Impact of Counteranion on Reversible Spin-State Switching in a Series of Cobalt(II) Complexes Containing a Redox-Active Ethylenedioxythiophene-Based Terpyridine Ligand

Subrata Ghosh, Abhishake Mondal, *et al.*

OCTOBER 20, 2022  
INORGANIC CHEMISTRY

READ 

### Iron-Catalyzed C–H Activation for Heterocoupling and Copolymerization of Thiophenes with Enamines

Takahiro Doba, Eiichi Nakamura, *et al.*

NOVEMBER 16, 2022  
JOURNAL OF THE AMERICAN CHEMICAL SOCIETY

READ 

### Oxygen versus Sulfur Coordination in Cobalt Superoxo Complexes: Spectroscopic Properties, O<sub>2</sub> Binding, and H-Atom Abstraction Reactivity

Jesse B. Gordon, David P. Goldberg, *et al.*

DECEMBER 20, 2022  
INORGANIC CHEMISTRY

READ 

### Ligand-Based Redox: Catalytic Applications and Mechanistic Aspects

Kirti Singh, Debashis Adhikari, *et al.*

OCTOBER 12, 2022  
ACS CATALYSIS

READ 

Get More Suggestions >